Limitations of Seasonal Predictability for Summer Climate over East Asia and the Northwestern Pacific*

YU KOSAKA

International Pacific Research Center, SOEST, University of Hawaii at Manoa, Honolulu, Hawaii

J. S. CHOWDARY

Indian Institute of Tropical Meteorology, Pune, India

SHANG-PING XIE

International Pacific Research Center, and Department of Meteorology, SOEST, University of Hawaii at Manoa, Honolulu, Hawaii

YOUNG-MI MIN

APEC Climate Center, Busan, South Korea

JUNE-YI LEE

International Pacific Research Center, SOEST, University of Hawaii at Manoa, Honolulu, Hawaii

(Manuscript received 30 December 2011, in final form 29 March 2012)

ABSTRACT

Predictability of summer climate anomalies over East Asia and the northwestern Pacific is investigated using observations and a multimodel hindcast ensemble initialized on 1 May for the recent 20–30 yr. Summertime East Asia is under the influence of the northwestern Pacific subtropical high (PASH). The Pacific–Japan (PJ) teleconnection pattern, a meridional dipole of sea level pressure variability, affects the northwestern PASH. The forecast models generally capture the association of the PJ pattern with the El Niño–Southern Oscillation (ENSO).

The Silk Road pattern, a wave train along the summer Asian jet, is another dominant teleconnection that influences the northwestern PASH and East Asia. In contrast to the PJ pattern, observational analysis reveals a lack of correlations between the Silk Road pattern and ENSO. Coupled models cannot predict the temporal phase of the Silk Road pattern, despite their ability to reproduce its spatial structure as the leading mode of atmospheric internal variability. Thus, the pattern is rather unpredictable at monthly to seasonal lead, limiting the seasonal predictability for summer in East Asia.

The anomalous summer of 2010 in East Asia is a case in point, illustrating the interference by the Silk Road pattern. Canonical anomalies associated with a decayed El Niño and developing La Niña would have the PJ pattern bring a cold summer to East Asia in 2010. In reality, the Silk Road pattern overwhelmed this tendency, bringing a record-breaking hot summer instead. A dynamical model experiment indicates that European blocking was instrumental in triggering the Silk Road pattern in the 2010 summer.

---

1. Introduction

The 2010 boreal summer marked a worldwide abnormal climate. A long-lived blocking high was established over eastern Europe, resulting in a drought that caused several hundred wildfires in western Russia (Grumm 2011). A severe flooding in late July affected about 20 million people in Pakistan with nearly 2000
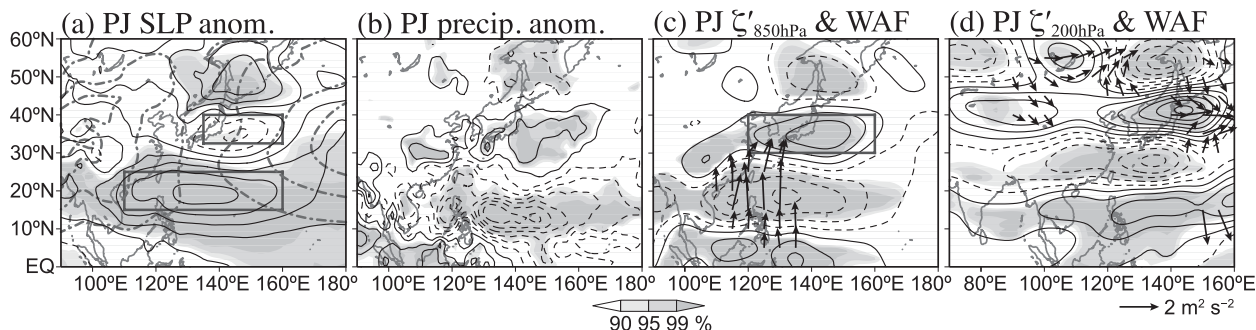
FIG. 1. Anomalies of (a) SLP, (b) precipitation, and (c) 850-hPa and (d) 200-hPa vorticity regressed onto the leading principal component of JJA 850-hPa vorticity over 10°–55°N, 100°–160°E based on the observational datasets. Contour intervals are (a) 0.2 (±0.1, ±0.3, ±0.5, …) hPa, (b) 0.4 (±0.2, ±0.6, ±1, …) mm day^{-1}, and (c),(d) 0.8 (±0.4, ±1.2, ±2, …) $\times 10^{-6}$ s^{-1}. Shading indicates corresponding confidence levels based on the t statistic. Dashed–dotted lines in (a) show climatological SLP for every 3 hPa. Arrows in (c),(d) indicate the wave-activity flux formulated by Takaya and Nakamura (2001) and evaluated with regressed anomalies. Boxes in (a),(c) correspond to areas where model prediction skill is evaluated in Table 1.

deaths (Houze et al. 2011). An unprecedented heat wave hit East Asia in July and August. The summer was the hottest in Japan since 1898 when record keeping began. An accurate prediction of such abnormal climates is important for economical activities, agriculture, and human lives.

Generally, the chaotic nature of the atmosphere precludes deterministic predictions longer than a few weeks. Seasonal predictions depend on oceanic anomalies of far longer time scales. Thus, the seasonal predictability is limited by the extent to which oceanic anomalies determine atmospheric variance.

Summertime East Asia is under the influence of the northwestern Pacific subtropical high (PASH)—the westward extension of the larger, basin-scale north PASH (see dashed–dotted lines in Fig. 1a). The El Niño–Southern Oscillation (ENSO) changes the intensity and location of the northwestern PASH, which in turn influences the East Asian summer climate. The ENSO generally peaks in boreal winter and influences the northwestern PASH both in its developing and decaying summers. The Pacific–Japan (PJ) pattern (Nitta 1987) is an important teleconnection that mediates ENSO influence on summertime East Asia (Xie et al. 2009; Kosaka et al. 2011). Figure 1 shows the PJ pattern extracted through an empirical orthogonal function (EOF) analysis applied to interannual variability of lower-tropospheric vorticity. The pattern is characterized by meridional dipoles of sea level pressure (SLP) and rainfall anomalies between the tropical (10°–25°N) and midlatitude (30°–40°N) northwestern Pacific (NWP).[1] Since

this dipole straddles the ridge of the climatological northwestern PASH over 25°–30°N (Fig. 1a), the pattern marks a meridional displacement as well as a westward expansion/eastward retreat of the high. Specifically, the PJ pattern, in the particular polarity shown in Fig. 1, displaces the northwestern PASH southwestward, bringing a cool (Wakabayashi and Kawamura 2004) and wet (Kosaka et al. 2011) summer to East Asia.

We have examined historical forecasts using several coupled general circulation models (GCMs) initialized on 1 May of each year. Table 1 evaluates skills of the model predictions by indicating correlations of ensemble-mean SLP with that in a reanalysis over the tropical and midlatitude lobes of the PJ pattern. The correlation for the tropical lobe is significantly high in all the models, at a typical value of 0.7. The high forecast skill suggests the dominant role of oceanic variability on the PJ tropical anomalies. In contrast, prediction skills in the midlatitude lobe are low and insignificant in all the models. The low skill in midlatitude predictions is confirmed by correlations of 850-hPa vorticity (Table 1). The present study investigates what limits the seasonal predictability for the summer mid-latitude NWP. Specifically, we examine how the ENSO influences seasonal predictability over the summer NWP, and the factors that limit predictability in midlatitude East Asia.

In addition to the PJ pattern, another dominant teleconnection called the Silk Road pattern (Enomoto et al. 2003; Enomoto 2004) is known to influence the strength and location of the northwestern PASH in boreal summer. Although it is suggested that both the PJ and Silk Road patterns are modes of atmospheric internal variability [Kosaka and Nakamura (2006, 2010) for the PJ pattern, and Sato and Takahashi (2006), Kosaka et al. (2009), and Ding et al. (2011) for the Silk Road pattern], our analysis shows that only the former is significantly correlated with, and thus modulated by, the ENSO. The Silk Road pattern

---

[1] Located north of these dipoles are additional SLP and rainfall anomalies, forming a tripolar anomaly pattern (Hirota and Takahashi 2012). The northernmost anomalies are beyond the scope of the present study.

TABLE 1. Coupled prediction models used in the present study. Periods indicate years analyzed statistically, in addition to the 2010 summer. Correlations of ensemble-mean JJA anomalies with those in JRA25 are also shown. Boldface indicates values exceeding 90% confidence level, based on the *t* statistic.

| | | | | | Correlations of JJA anomalies with those in JRA25 | | |
Acronym	Institution/model	Reference	Period	Ensemble size	SLP (15°–25°N, 110°–160°E)	SLP (32.5°–40°N, 135°–160°E)	850-hPa vorticity (30°–40°N, 120°–160°E)
NCEP CFS	National Centers for Environmental Prediction Climate Forecast System	Saha et al. (2006)	1981–2003	15	**0.71***	0.31	0.19
BMRC POAMA	Bureau of Meteorology Research Centre Predictive Ocean Atmosphere Model for Australia	Zhong et al. (2005)	1980–2002	10	**0.64***	0.10	0.24
FRCGC SINTEX-F	Frontier Research Center for Global Change Scale Interaction Experiment-FRCGC	Luo et al. (2005)	1982–2004	9	**0.77***	0.21	0.06
SNU	Seoul National University	Kug et al. (2008)	1980–2001	6	**0.73***	0.16	−0.16
JMA	Japan Meteorological Agency	Takaya et al. (2010)	1979–2008	5	**0.83***	0.11	0.12

* Confidence level exceeding 99%.

is much less predictable on the seasonal time scale and thereby reduces the seasonal predictability for the summer NWP. The 2010 hot summer in East Asia demonstrates this interference by the Silk Road pattern. The 2010 summer followed an El Niño event that peaked in the 2009/10 boreal winter, and featured a developing La Niña event. Both the decayed El Niño and developing La Niña brought seasonal predictability via the PJ pattern. The present study shows, however, that the Silk Road pattern overwhelmed the impact of the PJ pattern over East Asia and the midlatitude NWP. Our dynamical model experiment further indicates that the European blocking contributed to the 2010 hot summer in East Asia, illustrating the difficulty of seasonal predictions in summer.

The present study consists of statistical analyses and a case study for the 2010 summer, based on observational data and models. Section 2 describes the observational data and coupled model hindcasts/predictions used in the present study. Based on these data, section 3 discusses the seasonal predictability, with an emphasis on the PJ pattern. Motivated by a failure of seasonal predictions for the midlatitude NWP for the summer 2010, section 4 evaluates the extent to which the Silk Road pattern is predictable. Using a nonlinear dynamical model, section 5 examines the influence of the European blocking on the Silk Road pattern. Section 6 gives the conclusions. In this paper, seasons refer to those for the Northern Hemisphere.

2. Data and models

The present study uses monthly data of the Japanese 25-Year Reanalysis (JRA25) (Onogi et al. 2007), Climate Prediction Center (CPC) Merged Analysis of Precipitation (CMAP) (Xie and Arkin 1997), and the Met Office Hadley Centre Sea Ice and Sea Surface Temperature dataset (HadISST) (Rayner et al. 2003). Statistical analyses are performed for a 31-yr period from 1979 to 2009, together with the Niño-3.4 (5°S–5°N, 170°–120°W) sea surface temperature (SST) for November–January (NDJ) from 1978/79 to 2009/10.

Table 1 lists coupled general circulation models examined in the present study. These models have been used in the semioperational real-time long-lead coupled prediction of the Asian-Pacific Economic Cooperation (APEC) Climate Center (APCC) (Sohn et al. 2012) in cooperation with the Climate Prediction and its Application to Society (CliPAS) project (Wang et al. 2009; Lee et al. 2010). All of the models are initialized on 1 May of each year with ensemble sizes given in Table 1. The present study examines hindcasts for June–August (JJA) in the years listed in Table 1 and their 2010 summer predictions.

Since our statistical analysis concerns the ENSO, we must pay attention to its persistence when testing statistical significance. We evaluate the effective sample
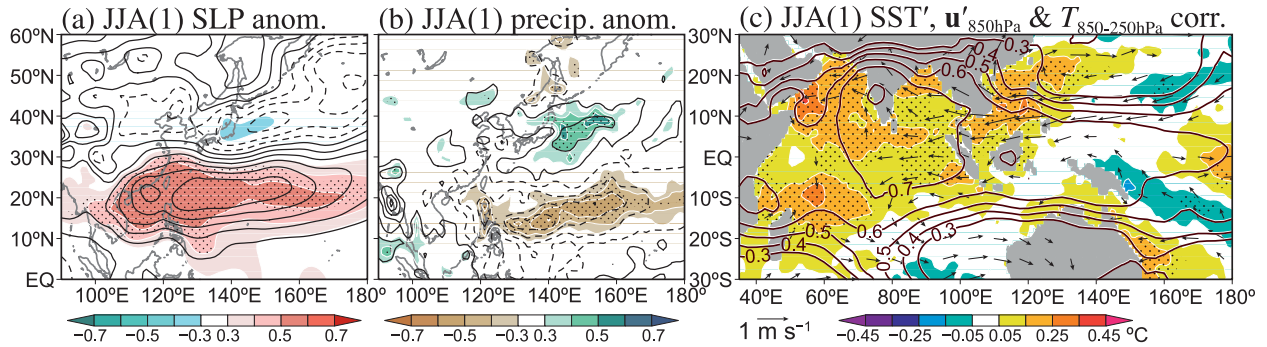
FIG. 2. Regressed anomalies and correlations for JJA against the Niño-3.4 SST in the preceding NDJ, based on the observational datasets: (a) SLP and (b) precipitation, where contours and shading indicate regressed anomalies and correlations, respectively, and (c) regressed anomalies of SST (shading) and 850-hPa wind (arrows) and correlations of tropospheric temperature (contours). Contour intervals for regressed anomalies are (a) 0.1 (± 0.05, ± 0.15, ± 0.25, …) hPa, (b) 0.4 (± 0.2, ± 0.6, ± 1, …) mm day^{-1}, and (c) 0.1 (± 0.05, ± 0.15, ± 0.25, …) °C, while correlations are plotted for ± 0.3, ± 0.4, ± 0.5, …. Stippling indicates confidence levels >95% for correlations of SLP, precipitation, and regressions of SST.

sizes N_{eff} for correlations/regressions of time series X and Y as

$$N_{\text{eff}} = RN/\max\left[1, 1 + 2\sum_{\tau=1}^{\tau_{\max}} (1 - \tau/N) r_X(\tau) r_Y(\tau)\right], \quad (1)$$

and for variance,

$$N_{\text{eff}} = RN \left/ \left[1 + 2\sum_{\tau=1}^{\tau_{\max}} (1 - \tau/N) r_X(\tau)^2\right]\right. \quad (2)$$

(Metz 1991; Livezey 1995). Here R denotes ensemble size ($R = 1$ for observation or model ensemble means), N represents data length, and $r_X(\tau)$ is an autocorrelation of time series X with a lag of τ years. For simplicity, the maximum lag $\tau_{\max}$ is set as the maximum number that does not exceed $N/2$.

Both observational and model hindcasts/prediction data are given on a 2.5° × 2.5° grid except HadISST, which has 1° × 1° resolution. To extract large-scale features, we applied a horizontal smoothing filter to relative vorticity by multiplying a spherical harmonic component of the total wavenumber n by $\exp\{-K[n(n + 1)]^2\}$ (Hoskins 1980) in which the coefficient K has been set in such a way that the harmonic component of $n = 24$ is reduced by 50% (Kosaka et al. 2009; Kosaka and Nakamura 2010). We evaluate a wave-activity flux formulated by Takaya and Nakamura (2001), which is parallel to local group velocities of stationary Rossby waves. Tropospheric temperature denotes temperature averaged between the 250-hPa and 850-hPa levels. We have repeated all of our statistical analyses based on linearly detrended data and obtained the same results qualitatively.

3. Predictability for the summer NWP via the PJ pattern

ENSO affects the NWP climate in both developing and decaying summers. This section first outlines such ENSO influences based on historical analysis and then discusses anomalies of the 2010 summer and their predictions.

a. The PJ pattern in summers following ENSO events

Figure 2 shows anomalies observed in summers following El Niño events. SLP and precipitation anomalies highlight a meridional dipole over the NWP (Figs. 2a,b), reminiscent of the PJ pattern (Fig. 1). This association between the decayed ENSO and the PJ pattern has been pointed out by Yang et al. (2007) and Xie et al. (2009). Since the PJ pattern in this particular polarity displaces the northwestern PASH southwestward, Fig. 2 suggests that a summer following an El Niño event tends to be cooler and wetter over the midlatitude NWP, including Japan.

The El Niño induces SST warming over the tropical Indian Ocean by changing net surface heat flux (Klein et al. 1999; Lau and Nath 2003; Tokinaga and Tanimoto 2004) and inducing downwelling oceanic Rossby waves in the southern basin (Xie et al. 2002; Huang and Kinter 2002). The Indian Ocean warming maximizes in boreal spring following El Niño, and continues into the following summer (Fig. 2c; Du et al. 2009) when SST anomalies have almost disappeared over the equatorial Pacific. The warmer Indian Ocean heats the troposphere and forces an equatorial Kelvin wave in the atmosphere (Fig. 2c), which extends into the western Pacific. Xie et al. (2009) proposed that this warm Kelvin wave is accompanied by surface Ekman convergence over the equatorial western Pacific, inducing surface divergence to its north over
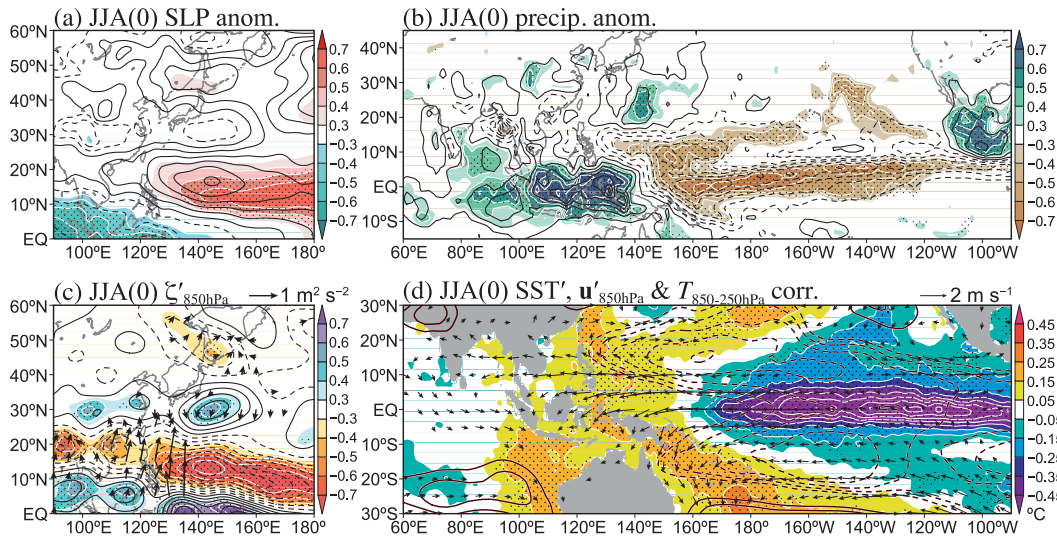
FIG. 3. Regressed anomalies and correlations for JJA against Niño-3.4 SST in the following NDJ based on the observational datasets. (a) SLP, (b) precipitation, and (c) 850-hPa vorticity, where contours and shading indicate regressed anomalies and correlations, respectively. (d) Regressed anomalies of SST (shading) and 850-hPa wind (arrows), and correlations of tropospheric temperature (contours). Signs are reversed to represent a typical La Niña–developing summer. Contour intervals of regressed anomalies are (a) 0.1 (± 0.05, ± 0.15, ± 0.25, ...) hPa, (b) 0.4 (± 0.2, ± 0.6, ± 1, ...) mm day^{-1}, (c) 0.4 (± 0.2, ± 0.6, ± 1, ...) $\times 10^{-6}$ s^{-1}, and (d) 0.1 (± 0.05, ± 0.15, ± 0.25, ...) °C. Correlations are plotted for ± 0.3, ± 0.4, ± 0.5, ... Arrows in (c) indicate the wave-activity flux calculated with regressed anomalies. Stippling indicates confidence levels >95% for correlations of SLP, precipitation, 850-hPa vorticity, and regressions of SST.

the tropical NWP and triggering the PJ pattern. Sui et al. (2007) and Wu et al. (2009) suggested that the local Hadley circulation anomaly associated with enhanced precipitation over the Maritime Continent suppresses atmospheric convection over the tropical NWP, forcing the PJ pattern.

b. Influence of developing ENSO on the summer NWP

The developing ENSO produces significant SST anomalies in summer and influences the NWP climate (Alexander et al. 2004). Figure 3 summarizes anomalies observed in La Niña–developing summers. We choose the polarity of La Niña rather than El Niño for its consistency with the 2010 summer case discussed later. The equatorial Pacific is significantly cooler, and a horseshoe pattern of warm anomalies prevails to its west (Fig. 3d). Rainfall decreases over the equatorial Pacific and increases over the Maritime Continent (Fig. 3b), representing an intensified Walker circulation. A precipitation increase is also observed around Central America.

Over the NWP, precipitation anomalies show a meridional dipole with dry and wet anomalies along 10°N and around 25°N, respectively (Fig. 3b). This dipole is accompanied by anomalously high (low) SLP over the tropical (midlatitude) NWP (Fig. 3a). Although the midlatitude SLP anomaly is insignificant (Fig. 3a), the

anomalous circulation is significantly cyclonic, as observed in lower-tropospheric vorticity anomalies (Fig. 3c). This SLP anomaly pattern represents an equatorward displacement of the northwestern PASH.

This SLP dipole has a certain projection onto the PJ pattern (Fig. 1a), although displaced southward. It is unclear how the developing ENSO induces this PJ-like meridional teleconnection in summer. We leave details of this mechanism for future investigations. Li and Wang (2005) and Wu et al. (2009) speculated that the cold Rossby wave response to La Niña over the tropical Pacific, as seen in a tropospheric temperature anomaly field (Fig. 3d), causes suppressed convection over the off-equatorial NWP (Fig. 3b), which may trigger the meridional teleconnection pattern.

c. 2010 summer anomalies and predictions

Summer 2010 was sandwiched between a preceding El Niño and a developing La Niña event. The Niño-3.4 SST anomalies were +1.40° and −1.64°C (+1.23 and −1.49 standard deviations) in NDJ 2009/10 and 2010/11, respectively. Figure 4 shows observed anomalies for JJA 2010. Here the climatology (means and interannual standard deviations) is derived from 1979–2009 seasonal-mean data.

SST was warmer than normal over the Indian Ocean, South China Sea, the Maritime Continent, and western
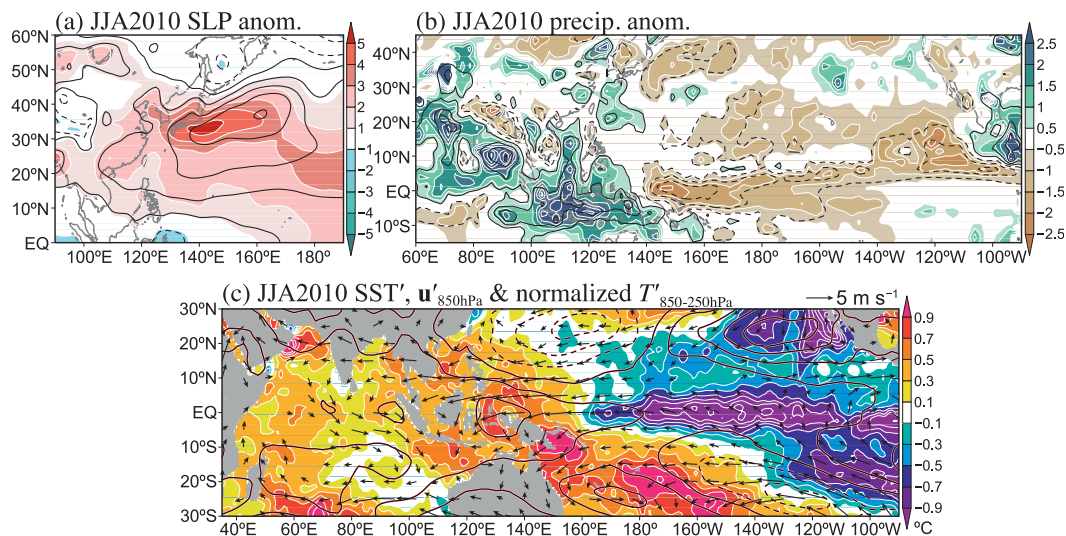
FIG. 4. Observed anomalies in JJA 2010: (a) SLP and (b) precipitation in contours, with shading representing the corresponding normalized anomalies; (c) SST (shading) and 850-hPa wind (arrows), and normalized anomalies of tropospheric temperature (contours). Contour intervals are 1 (± 0.5, ± 1.5, ± 2.5, ...) hPa, 2 (± 1, ± 3, ± 5, ...) mm day^{-1}, and 1 (± 0.5, ± 1.5, ± 2.5, ...).

Pacific and cooler over the equatorial and eastern Pacific (Fig. 4c). The overall distribution can be regarded as a combination of decayed El Niño (Fig. 2c) and developing La Niña (Fig. 3d) signals. Warming trends since the 1980s account for ~30% of the warm anomalies over the southwestern Pacific and equatorial Indian Ocean. Tropical precipitation anomalies in the 2010 summer (Fig. 4b) are largely consistent with those observed in La Niña–developing summers (Fig. 3b). Additionally, the Indian Ocean SST warming induced by the preceding El Niño (Figs. 2c, 4c) might contribute to rainfall increases over the northern Indian Ocean (Fig. 4b).

Ensemble predictions for the 2010 summer are summarized as multimodel ensemble (MME) mean anomalies in Fig. 5. The corresponding climatology is based on ensemble-mean data from individual models for 1982–2001, for which all model hindcasts are available. The models are successful in predicting SST anomalies and the zonally asymmetric distribution of precipitation anomalies in the tropics, except for an overestimation of precipitation increases along ~8°N over the western and central Pacific (Figs. 5b,c). Rainfall anomalies are somewhat weaker over the Maritime Continent and the equatorial Pacific. The overall successful prediction of tropical conditions derives from model skills in simulating ENSO, and illustrates that SST anomalies cause rainfall changes in the tropics. We expect the models to be able to capture the tropical influence on the extratropics qualitatively.

Our statistical analyses of historical data show that the NWP anomalies both in El Niño–decayed and La Niña–

developing summers feature a meridional SLP dipole with positive (negative) anomalies over the tropics (midlatitudes) (Figs. 2a, 3a). SST anomalies of both decayed El Niño and developing La Niña (Fig. 4c) force SLP anomalies over the NWP. Indeed, the coupled models predict such a SLP dipole, although the pattern is considerably displaced northeastward (Fig. 5a) compared to observations (Figs. 2a, 3a). Unexpected from the statistical and model predictions, positive SLP anomalies in the 2010 summer covered the entire NWP south of 45°N (Fig. 4a). This SLP monopole exceeds five standard deviations at its center. This anomaly pattern indicates an enhancement and northwestward expansion of the northwestern PASH, causing the record hot summer in East Asia. The failure of statistical and model predictions for this summer demonstrates the low seasonal predictability of summer climate over the midlatitude NWP shown in Table 1.

Compared to a typical summer following El Niño (Fig. 2c), the warm atmospheric Kelvin wave response shifted eastward in summer 2010 (Fig. 4c), possibly due to the warmer SST in the Maritime Continent region in addition to the Indian Ocean. Meanwhile, SST was cooler over the tropical North Pacific east of 170°E, associated with the developing La Niña. These conditions presumably resulted in an eastward-shifted rainfall decrease over the tropical NWP (Wu et al. 2010); the dry anomalies were, indeed, restricted east of 140°E between 10° and 25°N (Fig. 4b). The models reproduce the eastward-displaced precipitation decrease (Fig. 5b), resulting in an eastward-shifted PJ-like meridional
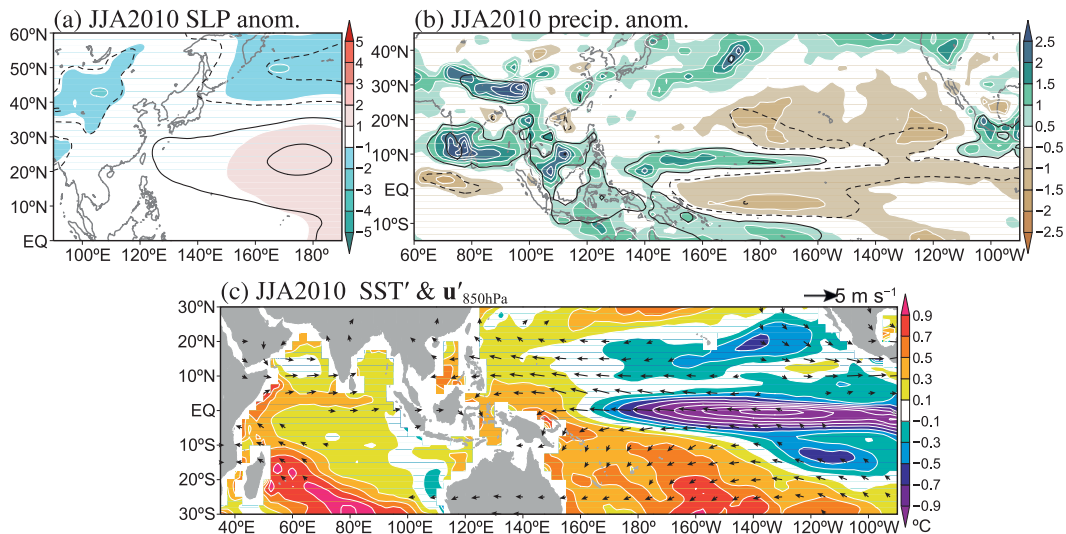
FIG. 5. As in Fig. 4 but for MME-mean anomalies in coupled model predictions. In (c) tropospheric temperature is not plotted owing to unavailability of the output. Climatology is derived from ensemble means of individual models for the period 1982–2001, for which all model hindcasts are available.

dipole (Fig. 5a). The larger meridional extent of the predicted PJ pattern is typical of model prediction (see the appendix). Through the PJ pattern, tropical anomalies would have induced negative SLP anomalies over the midlatitude NWP in this summer but, in reality, some other processes dominated the extratropical anomalies.

4. The Silk Road pattern and its seasonal predictability

The Silk Road teleconnection pattern influences the northwestern PASH (Enomoto et al. 2003; Enomoto 2004; Sato and Takahashi 2006; Kosaka et al. 2009). The pattern is characterized by a quasi-stationary Rossby wave train along the summer Asian jet, and can be regarded as the Eurasian part of the circumglobal teleconnection pattern in the Northern Hemisphere summer (Ding and Wang 2005). The pattern has an equivalent-barotropic structure with significant circulation anomalies reaching the lower troposphere to affect the northwestern PASH (Kosaka et al. 2009) and East Asian rainfall (Huang et al. 2011). Figures 6a,b show the Silk Road pattern extracted through an EOF analysis of the 200-hPa meridional wind velocity over the Asian jet region (30°–50°N, 30°–130°E) for JJA. The first and second EOF modes (EOF1 and EOF2) are wavelike anomalies with a common zonal wavenumber ~6 and their zonal phases displaced by nearly a quarter wavelength. EOF1 is well isolated from EOF2 based on the criteria by North et al. (1982), consistent with the zonal phase locking of the pattern (Kosaka et al. 2009).

The Silk Road pattern emerged in the 2010 summer with a vigorous amplitude. Two wave trains appeared

in the upper troposphere in July 2010, accompanied by eastward-directed wave-activity fluxes (Fig. 7a). One was along the polar front jet (65°–70°N) (Nakamura and Fukamachi 2004), including a strong anticyclone over eastern Europe that corresponds to a blocking high. The other aligned along the Asian jet (~40°N), with zonal wavenumber ~6 and zonal phases consistent with the Silk Road EOF1 pattern (Fig. 6a) east of 50°E. This Silk Road wave train continued into the following month with a slight retrogression of its zonal phase (Fig. 7b). Associated with this Silk Road wave train was an anomalous anticyclone over the midlatitude NWP, centered east of Japan in July and covering Japan in August (Figs. 7a,b). This anomalous anticyclone had nearly an equivalent-barotropic structure with a slight poleward phase tilt with height (figure not shown). It is thus likely that the Silk Road pattern induced the anomalous development of the surface northwestern PASH in summer 2010 (Fig. 4a). This section discusses predictions of the summer 2010 Silk Road pattern and seasonal predictability of the pattern.

a. The Silk Road pattern in coupled models and predictions for the 2010 summer

Figure 8 compares observed and predicted ensemble-mean anomalies of the upper-tropospheric circulation in the 2010 summer. Apparently, no model is successful in predicting the Silk Road pattern in the ensemble mean. Only in the SNU model, the predicted anomalies have comparable amplitudes (Fig. 8e), but the model shows a different wavelike structure aligned in the northwest–southeast direction over the Eurasian Continent.
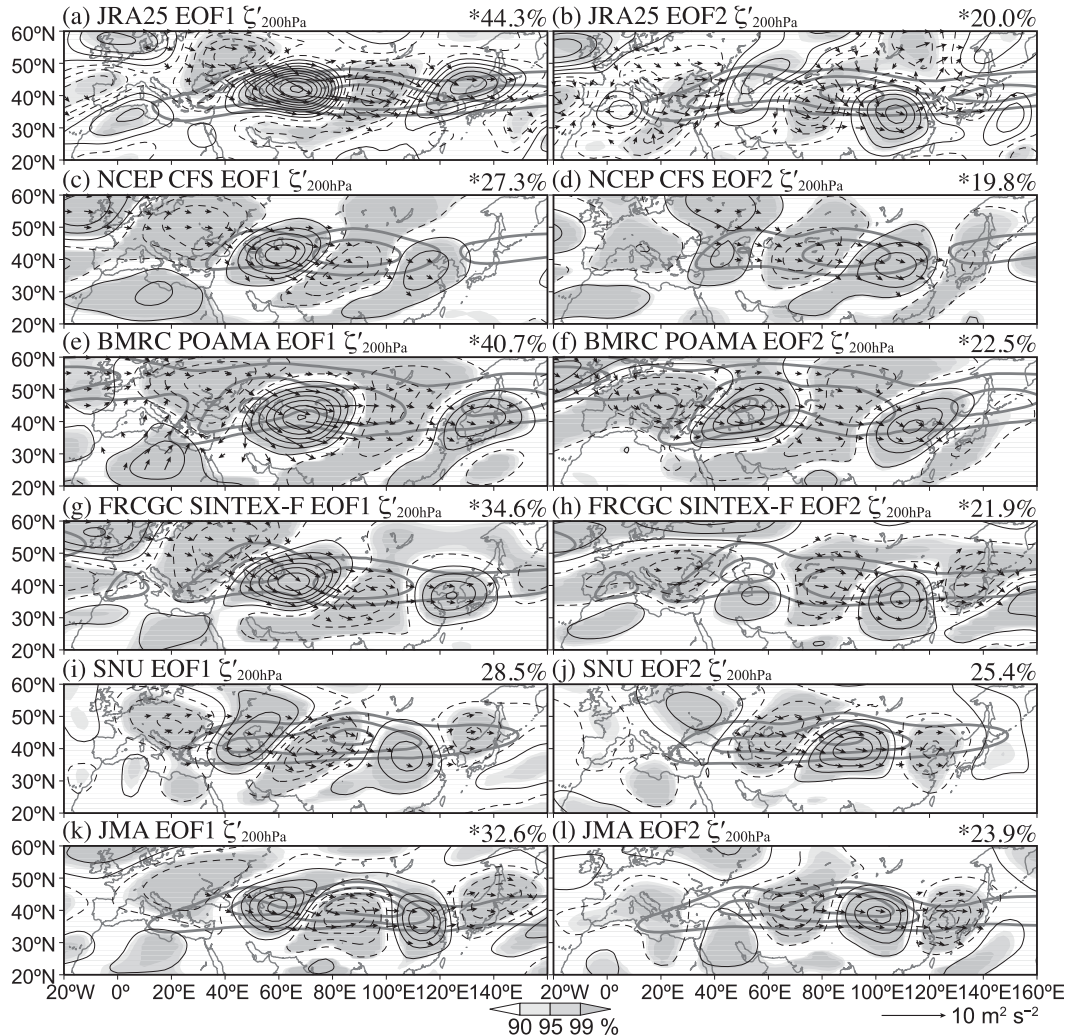
FIG. 6. The 200-hPa vorticity anomalies (thin solid and dashed contours) regressed onto the (left) leading and (right) second principal components of 200-hPa meridional wind velocity over 30°–50°N, 30°–130°E in JJA: (a),(b) JRA25, (c),(d) NCEP CFS, (e),(f) BMRC POAMA, (g),(h) FRCGC SINTEX-F, (i),(j) SNU, and (k),(l) JMA. Contour interval is 1 (±0.5, ±1.5, ±2.5, …) $\times 10^{-6}$ s^{-1}. Shading indicates corresponding confidence levels based on the t statistic. Thick lines show 20, 25, and 30 m s^{-1} contours of climatological zonal wind velocity. Arrows represent the wave-activity flux calculated with regressed anomalies. Variance fractions explained by the corresponding modes are denoted near the upper-right corner of each panel, with asterisks, if added, indicating that EOF1 and EOF2 are well isolated based on the criteria by North et al. (1982).

Actually, the SNU anomaly pattern is considerably different from observations (Fig. 8a) as well as the model's Silk Road pattern discussed later. The NCEP CFS, BMRC POAMA, and FRCGC SINTEX-F predict zonally elongated anomalies over the NWP (Figs. 8b–d), likely as upper-tropospheric manifestations of the PJ pattern (Fig. 1d). Consistent with our 2010 case, Lee et al. (2011) and Lee and Wang (2012) reported that the coupled models involved in the CliPAS project have difficulties in predicting the Silk Road pattern.

There are two possible reasons for models' failure in predicting the Silk Road pattern. First, the models are

unable to reproduce the Silk Road pattern as a mode of internal variability. Second, the temporal phase of the Silk Road pattern is unpredictable as represented in model ensemble means with the present initialization systems.

To examine the first possibility, the same EOF analysis as applied to the observations (Figs. 6a,b) is repeated with the model hindcast archive (Figs. 6c–l). Note that the ensemble mean is not taken before the EOF analysis: anomalies include both the ensemble-mean and inter-member variability. All of the models successfully reproduce midlatitude wave trains as the leading modes
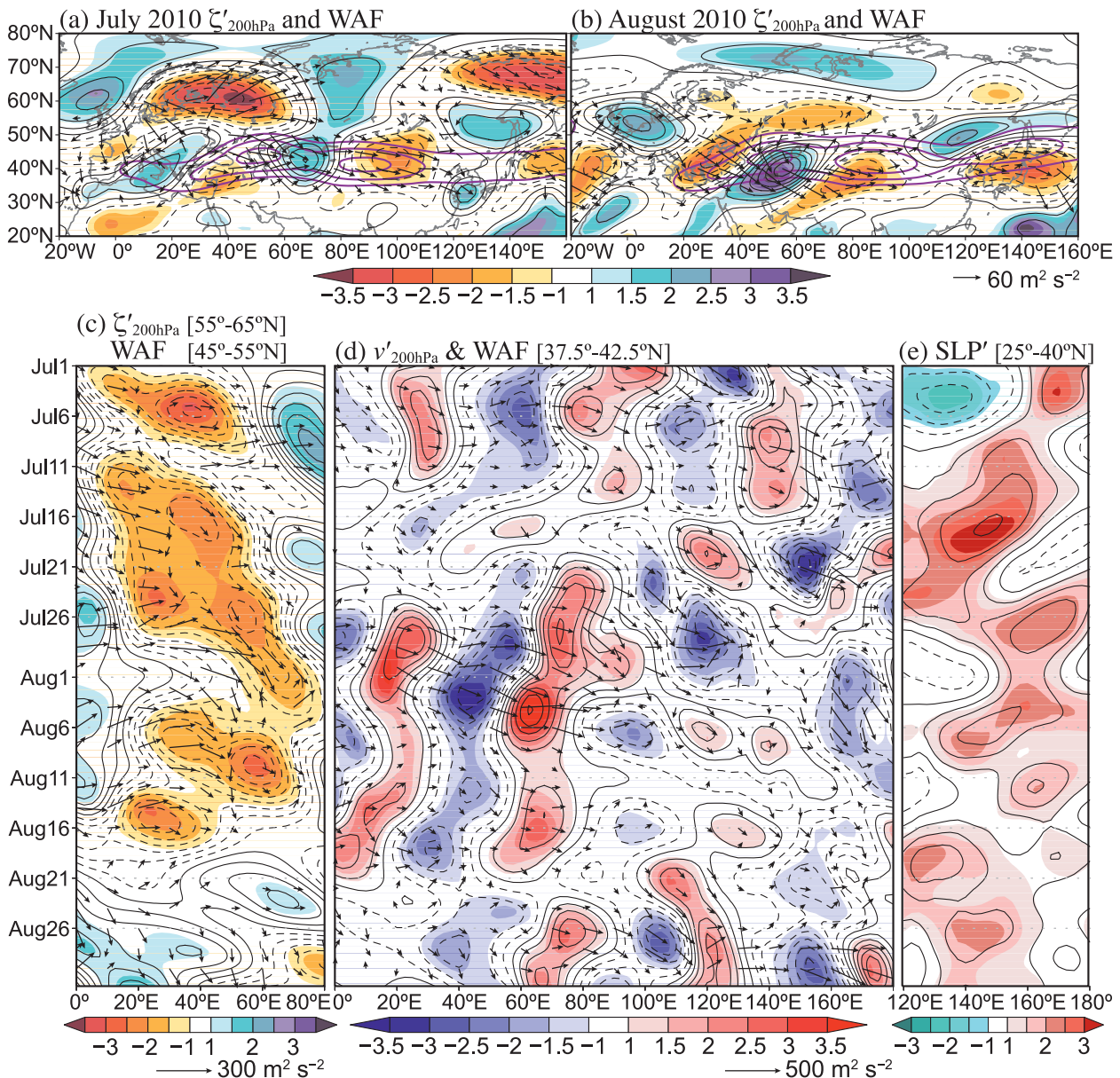
FIG. 7. Anomalies (black contours) and normalized anomalies (shading) observed in July–August 2010: 200-hPa vorticity anomalies for (a) July and (b) August 2010. Low-pass filtered anomalies from 1 Jul to 31 Aug 2010 with a cutoff period of 8 days for (c) 200-hPa vorticity averaged for 55°–65°N; (d) 200-hPa meridional wind averaged for 37.5°–42.5°N, and (e) SLP averaged for 25°–40°N. Arrows show horizontal component of the 200-hPa wave-activity flux in July and August 2010, (c) averaged for [45°–55°N], and (d) averaged for [37.5°–42.5°N]. Contour intervals are $6 \, (\pm 3, \pm 9, \pm 15, \ldots) \times 10^{-6} \, \text{s}^{-1}$, $5 \, (\pm 2.5, \pm 7.5, \pm 12.5, \ldots) \, \text{m s}^{-1}$, and $2 \, (\pm 1, \pm 3, \pm 5, \ldots)$ hPa. Purple lines in (a),(b) indicate 20, 25, and 30 m s^{-1} contours of climatological zonal wind velocity.

(Figs. 6c–l), albeit with reduced amplitudes compared to the observed EOF1 (Fig. 6a). Except for the SNU model, EOF1 is well isolated from EOF2 based on the North et al. (1982) criteria with N_{eff} degrees of freedom obtained from Eq. (2), indicative of the zonal phase anchoring. The exact zonal phase varies among models. The FRCGC SINTEX-F exhibits surprisingly high reproducibility of the structure of the Silk Road pattern

with spatial correlations ~0.9 (Table 2). Thus model failure in predicting the 2010 Silk Road pattern is not due to that in reproducing the pattern as the internal mode.

Table 2 evaluates the signal-to-noise (S/N) ratios of principal components (PCs), defined as variance of the ensemble-mean PC divided by intermember variance of the PC. S/N = 1 indicates that ensemble-mean
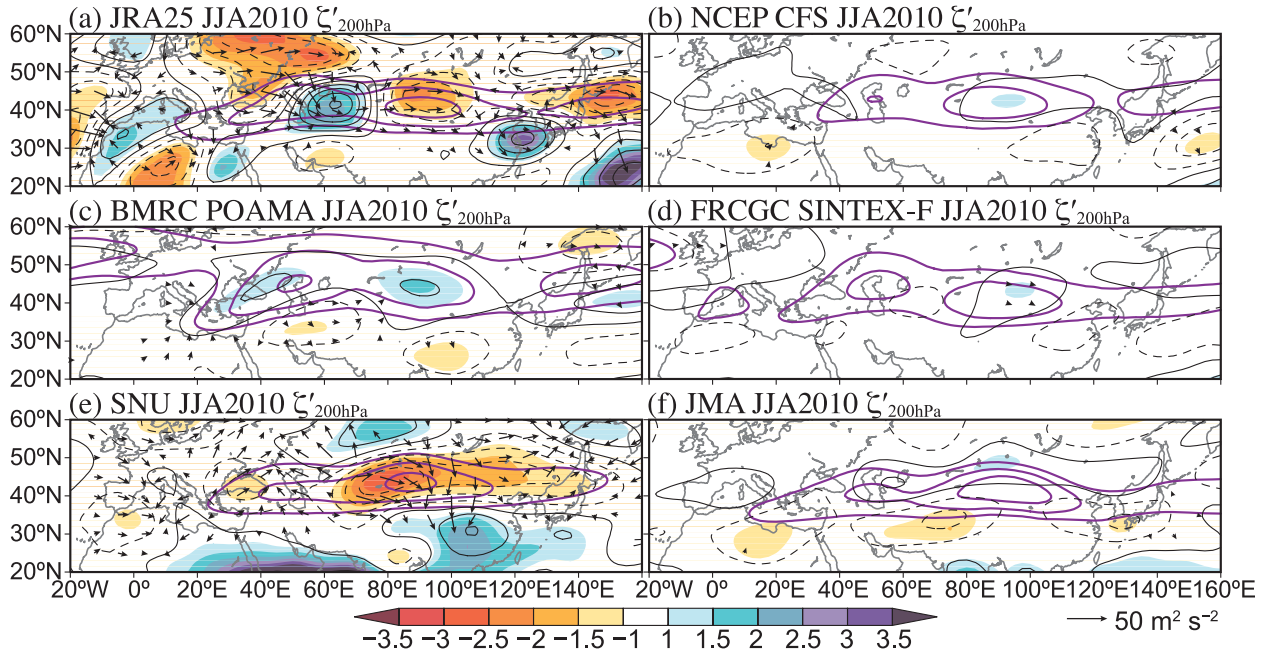
FIG. 8. (a) Observed and (b)–(f) predicted ensemble-mean anomalies of 200-hPa vorticity in JJA 2010 (black contours): contour interval $4 (\pm2, \pm6, \pm10, \dots) \times 10^{-6}$ s^{-1}. Shading shows anomalies normalized by climatological standard deviation [including intermember variability in (b)–(f)]. Purple lines indicate 20, 25, and 30 m s^{-1} contours of climatological zonal wind velocity. Arrows indicate the associated wave-activity flux.

anomalies have the same amplitude as the ensemble spread. For S/N < 1, the prediction becomes unreliable. By definition, the S/N ratio tends to decrease as model ensemble size increases (Table 2). Typically, the S/N ratio is low (0.1 ~ 0.3), indicating that the temporal phase of the Silk Road pattern is rather unpredictable. In many models, PCs cannot be distinguished from a white noise based on statistical insignificance derived from the Monte Carlo method. These results support the second possibility mentioned above: the models with their initialization systems cannot predict the temporal phase of the Silk Road pattern, despite their ability for the spatial pattern as the internal mode.

b. The observed Silk Road pattern and ENSO

The unpredictability of the temporal phase of the Silk Road pattern suggests that oceanic variability does not effectively force the pattern. The present subsection examines relationships of the Silk Road pattern to SST anomalies including ENSO, based on historical observations. Since at the present stage we do not know any preferred phases of the Silk Road pattern forced by ENSO, we allow for a linear combination of observational EOF1 (Fig. 6a) and EOF2 (Fig. 6b):

$$\xi = \sqrt{\lambda_1}\hat{\xi}_1 \cos\theta + \sqrt{\lambda_2}\hat{\xi}_2 \sin\theta. \qquad (3)$$

TABLE 2. Summary of EOF1 and EOF2 for JJA 200-hPa meridional wind velocity over 30°–50°N, 30°–130°E: pattern correlations with observational counterparts, and the S/N ratios measured as variance of the ensemble-mean PC divided by intermember variance of PC. The S/N ratio is shown in boldface if the ensemble can be significantly distinguished from white noise at the confidence level of 90%, based on a Monte Carlo method with the same ensemble size and N_{eff}/R length.

Model	Pattern correlation with JRA25 EOFs		S/N ratio as (ensemble mean/intermember) PC variance		
	EOF1	EOF2	PC1	PC2	PC1 + PC2
NCEP CFS	0.73	0.62	0.08	0.05	0.07
BMRC POAMA1.5	0.90	0.79	**0.22****	**0.18***	**0.20***
FRCGC SINTEX-F	0.96	0.89	0.07	**0.20**	0.11
SNU	0.38	0.28	0.13	**0.34***	0.22
JMA	0.42	0.53	**0.42***	0.35	**0.39**

 * Confidence level 99%.
** Confidence level 95%.
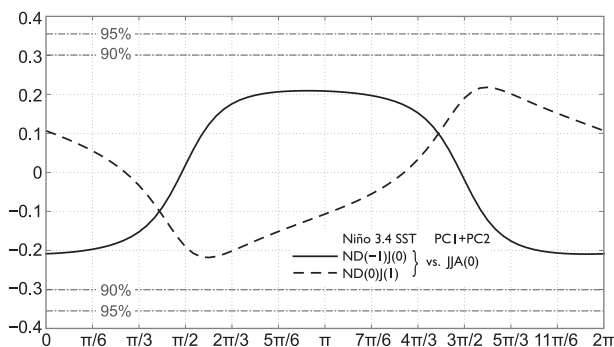
FIG. 9. Correlations of the linear combinations of the leading and second observational PCs for 200-hPa meridional wind over 30°–50°N, 30°–130°E for JJA with Niño-3.4 SST in preceding and following NDJs. Abscissa indicates θ in Eq. (3). Solid (dashed) lines correspond to the preceding (following) NDJ for the Niño-3.4 index. Dashed–dotted lines represent confidence levels as indicated, based on the t statistic ($N_{\text{eff}} = N$ for all θ).

Here $\hat{\xi}_i$ denotes the ith nondimensional EOF pattern and λ_i the ith eigenvalue. By changing θ we permit arbitrary zonal phases of the Silk Road pattern as ξ. One can easily show that the corresponding time series also derives from Eq. (3) by regarding $\hat{\xi}_i$ as the ith normalized PC.

Figure 9 shows correlations of the combined PC with Niño-3.4 SST in preceding and following winters. Correlations are lower than ~0.2 for all θ and do not attain the 90% significance level with $N_{\text{eff}} = N$. Therefore, the Silk Road pattern does not significantly correlate with ENSO. This result suggests that models' inability to predict the phase of the Silk Road pattern is due to the nature of the pattern as an internal mode *unforced* by the ocean.

ENSO actually induces significant circulation anomalies in its decay summers over the Eurasian Continent. A regression map, shown in Fig. 10a, reveals that the anomalies are incoherent and out of phase with the Silk Road pattern observed in summer 2010. The NWP anomalies are associated with the PJ pattern (Fig. 1d). In

ENSO-developing summers, circulation anomalies are restricted to Europe and West Asia (Fig. 10b). The absence of organized zonal wave trains in Fig. 10 is consistent with our result in Fig. 9.

Correlation maps between the Silk Road PCs and SST anomalies confirm the absence of associations between the Silk Road pattern and ENSO (Fig. 11). Neither EOF1 nor EOF2 are accompanied by any significant SST anomalies over the equatorial Pacific and Indian Ocean (Fig. 11). Cooler SST over the equatorial eastern Pacific in EOF2 is largely insignificant (Fig. 11b). The correlation is significant over the subtropical North Atlantic and Caribbean Sea in EOF1 (Fig. 11a). While causality of these SST anomalies and the Silk Road pattern is unresolved at this point, the correlations may indicate a weak potential predictability of the latter. Yet, the weak or nonassociation of the Silk Road pattern with major SST modes is consistent with the result from coupled model hindcasts (section 4a), suggesting seasonal unpredictability of the pattern.

5. Influence of the European blocking in the 2010 summer

The 2010 summer marked a strong blocking event over eastern Europe (Grumm 2011). In Fig. 7a, the wave-activity flux emanates from the blocking anticyclone, with a southward component on the southern periphery (Fig. 7c). Following intensification of the blocking (Fig. 7c), anomalous wave trains, stationary in zonal phases, formed with eastward group velocity along the Asian jet (Fig. 7d), leading to an enhanced northwestern PASH (Fig. 7e). Thus, the possibility is suggested that the blocking anticyclone fed the Silk Road pattern in summer 2010.

The present section examines this possibility by using a nonlinear baroclinic model (NLBM) based on a dry atmospheric general circulation model used in Watanabe (2009) and Yasui and Watanabe (2010). The horizontal
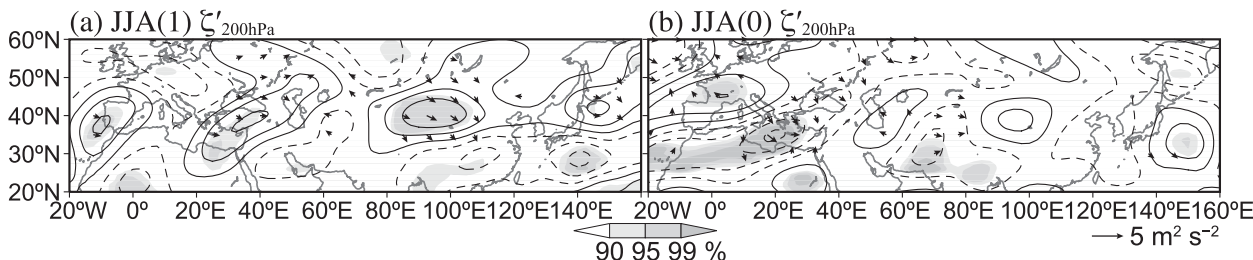
FIG. 10. The 200-hPa vorticity anomalies regressed onto Niño-3.4 SST in the (a) preceding and (b) following NDJ based on the observational data. In (b) signs are reversed to represent the La Niña–developing summer. Contour interval is 1 ($\pm0.5, \pm1.5, \pm2.5, \ldots$) $\times$ 10^{-6} s^{-1}. Arrows indicate the wave-activity flux calculated with regressed anomalies; shading represent corresponding confidence levels based on the t statistic.
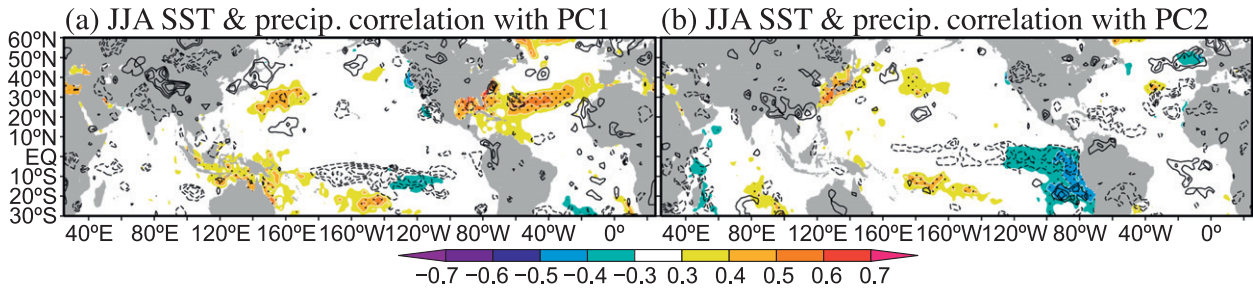
FIG. 11. Correlations of SST (shading) and precipitation (contours) with the (a) leading and (b) second PCs of the 200-hPa meridional wind velocity over 30°–50°N, 30°–130°E in JJA based on the observational data. Contours are plotted for ±0.3, ±0.4, ±0.5, ... Stippling indicates confidence levels >95% for correlations of SST.

resolution is T42 with 20 σ layers in the vertical. The model includes biharmonic horizontal diffusion with e-folding time of 1 day for the smallest wave.

The NLBM is initialized with July climatology derived from the JRA25. In our control experiment this initial state is sustained by artificial forcing, which has been obtained as sign-reversed quantities of one time step changes in temperature, vorticity, divergence, and surface pressure in an unforced experiment. In addition to this artificial forcing to maintain the initial state, our sensitivity experiment prescribes a hypothetical vorticity forcing, whose horizontal distribution and vertical profile are shown in Figs. 12a,b, to mimic the blocking anticyclone as its response. A response to the vorticity forcing is defined as the difference between the two experiments averaged from day 11 to 20. Actually, the result is almost unchanged if we adopt differences from the initial state as the response since drift in the control experiment is weak.

Figure 12c shows the response to the vorticity forcing. In addition to an anticyclonic perturbation over eastern Europe and an associated wave train along the polar front jet, a wave train develops along the Asian jet. Although an anticyclonic perturbation over 80°–110°E is too strong, the wave train has zonal phases consistent with those observed in July 2010 (Fig. 7a), accompanying an anomalous anticyclone centered just east of Japan (Fig. 12c). The NLBM experiment indicates that the blocking high over eastern Europe contributed to the development of the Silk Road pattern in the 2010 summer. This result is consistent with the Hong et al. (2011) observational analysis that the cyclonic anomaly centered south of the Aral Sea (~45°N, 60°E) in summer 2010 (Figs. 7a,b and 8a) was induced by the blocking, causing the severe flood in Pakistan. The cyclonic anomaly can be regarded as a part of the Silk Road pattern.

We have also conducted additional experiments with the vorticity forcing displaced eastward/westward by 5° and 10° and northward/southward by 5°. The Silk Road wave trains have almost the same structure and amplitude as shown in Fig. 12c, consistent with the zonal phase locking of the pattern (Kosaka et al. 2009).

Since blocking phenomena owe their existence largely to atmospheric nonlinear dynamics, their seasonal prediction is highly difficult (Dole et al. 2011). Matsueda (2011) showed that the summer 2010 blocking was
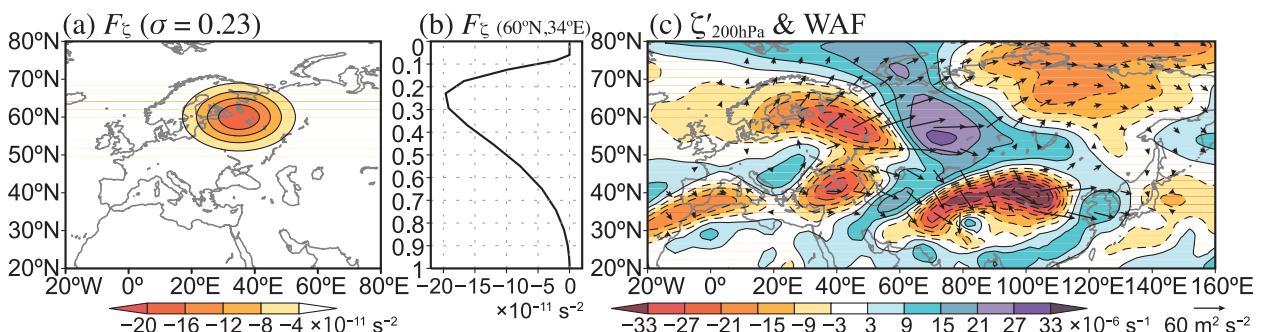
FIG. 12. (a) The horizontal distribution at $\sigma = 0.23$ and (b) vertical profile at 60°N, 33.8°E of stationary vorticity forcing prescribed to the NLBM. (c) Response of the NLBM to the vorticity forcing, shown in (a),(b), initialized with July climatology. Contours and shading show 200-hPa vorticity perturbations, while arrows indicate the wave-activity flux evaluated from zonally asymmetric perturbation of 200-hPa streamfunction. Contour intervals are 4×10^{-11} s^{-2} in (a) and $6 \ (\pm 3, \pm 9, \pm 15, \ldots) \times 10^{-6}$ s^{-1} in (c).

predictable at a lead time of 9 days—too short for seasonal predictions. This is consistent with our results in section 4 that the seasonal prediction skills for the Silk Road pattern are low in general.

While our experiment demonstrates that blocking is an effective trigger of the Silk Road pattern, Yasui and Watanabe (2010) showed that optimum thermal forcing for the Silk Road pattern is distributed globally, including that associated with Indian monsoon anomalies (Ding and Wang 2005). However, an experiment using the linear version of NLBM (Watanabe and Kimoto 2000) forced with the JRA25 diabatic heating anomalies in July 2010 was unsuccessful in reproducing the observed Silk Road pattern (figure not shown). This result further highlights the importance of European blocking in the 2010 summer.

6. Conclusions and discussion

The PJ (Fig. 1) and the Silk Road (Fig. 6) patterns are the major teleconnections that change the location and strength of the northwestern PASH and thereby influence East Asian climate in summer. Correlations of the PJ pattern with decayed (Fig. 2) and developing (Fig. 3) ENSO suggest its seasonal predictability. Indeed, the coupled models that have participated in the CliPAS project demonstrate their ability to predict the tropical lobe of the PJ meridional dipole (Table 1, Chowdary et al. 2010). The seasonal predictability is low in the midlatitude lobe of the PJ pattern because of unpredictability of the Silk Road pattern. This low seasonal predictability comes from the lack of significant correlations between the Silk Road pattern and both developing and decayed ENSO (Figs. 9, 10). In fact, the coupled models cannot predict the temporal phase of the Silk Road pattern in their ensemble means (Table 2), despite their ability to reproduce the spatial pattern as the leading mode of internal variability (Fig. 6). Thus, the seasonal prediction of the Silk Road pattern remains challenging.

The anomalous summer 2010 demonstrates this interference of the Silk Road pattern over East Asia. Summer 2010 followed an El Niño event and preceded the peak of a La Niña event, bringing seasonal predictability to the PJ pattern. Both our statistical analysis and coupled models predict a southward shift of the northwestern PASH, which would have brought an anomalously cold summer to East Asia (Figs. 2, 3, and 5). However, the actual summer 2010 anomalies were the opposite of this prediction, featuring an enhancement and northwestward expansion of the northwestern PASH that caused a record-breaking hot summer in East Asia (Fig. 4). The noncanonical development of the northwestern PASH

was caused by the Silk Road pattern that overwhelmed the PJ midlatitude anomalies (Fig. 7). None of the coupled models successfully predicted the temporal phase of the Silk Road pattern (Fig. 8), consistent with its seasonal unpredictability. The large internal variability in the Silk Road pattern calls for a probabilistic forecast for East Asia, with uncertainty estimates derived from multimodel and multimember predictions.

Our NLBM experiment suggests that the blocking, developed over eastern Europe, was instrumental in triggering the Silk Road pattern in the 2010 summer (Fig. 12) (Hong et al. 2011). Blocking events are generally unpredictable beyond one to two weeks, as was the case for the summer 2010 blocking (Dole et al. 2011; Matsueda 2011), illustrating the intrinsic challenge in predicting the 2010 summer Silk Road pattern. The experiment demonstrates that the Silk Road pattern can develop from nonlinear behavior of the dynamical atmosphere, in addition to diabatic heating (Yasui and Watanabe 2010). Both processes contribute to the large intermember variance of the Silk Road pattern.

If the PJ pattern dominated the midlatitude NWP and were determined by anomalies in the tropics, the summer climate in East Asia would be highly predictable. The present study shows that the interference by the Silk Road pattern, which is of low predictability on the seasonal time scale, makes it difficult to predict the East Asian summer climate even though the anomalies in the PJ tropical lobe are highly predictable. Hsu and Lin (2007) indicated that the Silk Road pattern is more effective in inducing dry and warm than wet and cool conditions in East Asia, an asymmetry that might further complicate the summer 2010 predictions.

It should be noted that the high predictability of the PJ tropical lobe would not be attained if the prediction models were decoupled from the ocean. Precipitation correlates negatively with local SST over the tropical NWP in summer (Wang et al. 2005) (cf. Figs. 2b,c also). In atmospheric general circulation models with prescribed SST, convection is rather sensitive to the local SST, yielding unrealistic precipitation in the PJ tropical lobe (Wang et al. 2004; Wu and Kirtman 2007). Indeed, AGCMs show low skill in predicting summer NWP variability (Kang and Shukla 2006; Zhou et al. 2009). Coupled models are therefore crucial for predictions of the PJ pattern (Chowdary et al. 2010).

Complicating the issue of predictability, the midlatitude lobe of the PJ pattern is sensitive to local precipitation anomalies (Lu and Lin 2009), not simply a passive response to tropical anomalies, as a casual inspection of the PJ pattern might imply. This indicates a positive feedback between latent heating and circulation. Models are known to have a problem in simulating
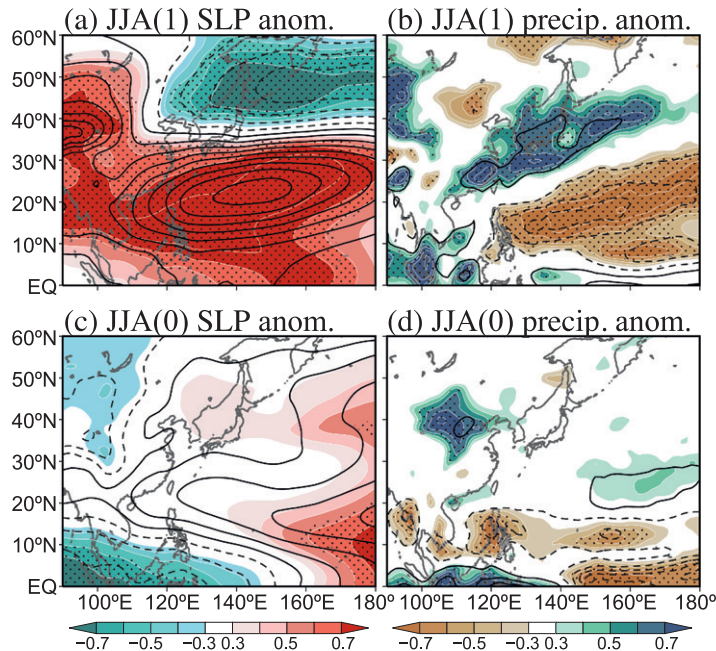
FIG. A1. Regressed anomalies (contours) and correlations (shading) of (a), (c) SLP and (b),(d) precipitation for JJA against observed Niño-3.4 SST in the (a),(b) preceding and (c),(d) following NDJ, based on the MME-mean hindcasts for 1982–2001. In (c),(d) signs are reversed to represent the La Niña–developing summer. Contour intervals for regressed anomalies are 0.1 (± 0.05, ± 0.15, ± 0.25, ...) hPa and 0.4 (± 0.2, ± 0.6, ± 1, ...) mm day^{-1}, while correlations are plotted for ± 0.3, ± 0.4, ± 0.5, ... Stippling indicates confidence levels >95% for correlations.

the mei-yu/baiu rainband (Ninomiya et al. 2002; Ninomiya 2009). Thus, low skill in predicting variability in the PJ midlatitude lobe might be due partly to model inability to simulate the feedback between latent heating and circulation. Recent studies show that the mei-yu/baiu rainfall develops in a favorable large-scale dynamical environment, in particular in response to warm advection by the Asian jet in the midtroposphere (Sampe and Xie 2010; Kosaka et al. 2011). Increased resolution in general circulation models appears to help improve their skills in simulating the mei-yu/baiu rainband (Kawatani and Takahashi 2003; Lau and Ploshay 2009) and thereby latent heating–circulation feedback. In addition, the coupled models examined in the present study show an unrealistically large meridional extent of the PJ pattern (Fig. 5a, also see the appendix), leaving room for model improvements. Progress in these areas holds promise of improving predictability in the East Asian summer via the PJ teleconnection pattern.

APPENDIX

Reproducibility of the PJ Pattern in the Models

Chowdary et al. (2010) showed considerable skill of coupled models in reproducing the PJ tropical lobe of SLP in an ENSO-decay summer (Fig. A1a). The models are also able to predict the precipitation dipole (Fig. A1b). However, the midlatitude lobe of SLP anomalies exhibits a poleward displacement (Fig. A1a) compared to observations (Fig. 2a). The EOF analysis, as applied to observations in Fig. 1, also reveals an unrealistically large meridional extent of the PJ SLP dipole

in the models (figure not shown). This model bias is consistent with their prediction for the 2010 summer (Fig. 5a). For the ENSO-developing summer, the SLP and rainfall anomalies are overall reproduced (Figs. A1c,d), although the midlatitude negative anomalies in SLP diminish (cf. with Fig. 3a). The model deficiencies in reproducing the midlatitude NWP anomalies might have worsened the East Asian summer prediction, which can potentially be corrected by model improvements.

REFERENCES

Alexander, M. A., N.-C. Lau, and J. D. Scott, 2004: Broadening the atmospheric bridge paradigm: ENSO teleconnections to the tropical West Pacific-Indian Oceans over the seasonal cycle and to the North Pacific in summer. *Earth's Climate: The Ocean-Atmosphere Interaction, Geophys. Monogr.,* Vol. 147, Amer. Geophys. Union, 85–103.

Chowdary, J. S., S.-P. Xie, J.-Y. Lee, Y. Kosaka, and B. Wang, 2010: Predictability of summer northwest Pacific climate in 11 coupled model hindcasts: Local and remote forcing. *J. Geophys. Res.,* **115,** D22121, doi:10.1029/2010JD014595.

Ding, Q., and B. Wang, 2005: Circumglobal teleconnection in the Northern Hemisphere summer. *J. Climate,* **18,** 3483–3505.

——, and ——, J. M. Wallace, and G. Branstator, 2011: Tropical–extratropical teleconnections in boreal summer: Observed interannual variability. *J. Climate,* **24,** 1878–1896.

Dole, R., and Coauthors, 2011: Was there a basis for anticipating the 2010 Russian heat wave? *Geophys. Res. Lett.,* **38,** L06702, doi:10.1029/2010GL046582.

Du, Y., S.-P. Xie, G. Huang, and K. Hu, 2009: Role of air–sea interaction in the long persistence of El Niño–induced north Indian Ocean warming. *J. Climate,* **22,** 2023–2038.

Enomoto, T., 2004: Interannual variability of the Bonin high associated with the propagation of Rossby waves along the Asian jet. *J. Meteor. Soc. Japan,* **82,** 1019–1034.

——, B. J. Hoskins, and Y. Matsuda, 2003: The formation mechanism of the Bonin high in August. *Quart. J. Roy. Meteor. Soc.,* **129,** 157–178.

Grumm, R. H., 2011: The central European and Russian heat event of July–August 2010. *Bull. Amer. Meteor. Soc.,* **92,** 1285–1296.

Hirota, N., and M. Takahashi, 2012: A tripolar pattern as an internal mode of the East Asian summer monsoon. *Climate Dyn.,* doi:10.1007/s00382-012-1416-y, in press.

Hong, C.-C., H.-H. Hsu, N.-H. Lin, and H. Chiu, 2011: Roles of European blocking and tropical-extratropical interaction in the 2010 Pakistan flooding. *Geophys. Res. Lett.,* **38,** L13806, doi:10.1029/2011GL047583.

Hoskins, B. J., 1980: Representation of the earth topography using spherical harmonics. *Mon. Wea. Rev.,* **108,** 111–115.

Houze, R. A., K. L. Rasmussen, S. Medina, S. R. Brodzik, and U. Romatschke, 2011: Anomalous atmospheric events leading to the summer 2010 floods in Pakistan. *Bull. Amer. Meteor. Soc.,* **92,** 291–298.

Hsu, H.-H., and S.-M. Lin, 2007: Asymmetry of the tripole rainfall pattern during the East Asian summer. *J. Climate,* **20,** 4443–4458.

Huang, B., and J. L. Kinter III, 2002: Interannual variability in the tropical Indian Ocean. *J. Geophys. Res.,* **107,** 3199, doi:10.1029/2001JC001278.

Huang, G., Y. Liu, and R. H. Huang, 2011: The interannual variability of summer rainfall in the arid and semiarid regions of northern China and its association with the northern hemisphere circumglobal teleconnection. *Adv. Atmos. Sci.,* **28,** 257–268.

Kang, I.-S., and J. Shukla, 2006: Dynamic seasonal prediction and predictability of the monsoon. *The Asian Monsoon,* B. Wang, Ed., Springer Praxis, 585–612.

Kawatani, Y., and M. Takahashi, 2003: Simulation of the Baiu front in a high resolution AGCM. *J. Meteor. Soc. Japan,* **81,** 113–126.

Klein, S. A., B. J. Soden, and N.-C. Lau, 1999: Remote sea surface temperature variations during ENSO: Evidence for a tropical atmospheric bridge. *J. Climate,* **12,** 917–932.

Kosaka, Y., and H. Nakamura, 2006: Structure and dynamics of the summertime Pacific-Japan teleconnection pattern. *Quart. J. Roy. Meteor. Soc.,* **132,** 2009–2030.

——, and ——, 2010: Mechanisms of meridional teleconnection observed between a summer monsoon system and a subtropical anticyclone. Part I: The Pacific–Japan pattern. *J. Climate,* **23,** 5085–5108.

——, ——, M. Watanabe, and M. Kimoto, 2009: Analysis on the dynamics of a wave-like teleconnection pattern along the summertime Asian jet based on a reanalysis dataset and climate model simulations. *J. Meteor. Soc. Japan,* **87,** 561–580.

——, S.-P. Xie, and H. Nakamura, 2011: Dynamics of interannual variability in summer precipitation over East Asia. *J. Climate,* **24,** 5435–5453.

Kug, J.-S., I.-S. Kang, and D.-H. Choi, 2008: Seasonal climate predictability with tier-one and tier-two prediction system. *Climate Dyn.,* **31,** 403–416.

Lau, N.-C., and M. J. Nath, 2003: Atmosphere–ocean variations in the Indo-Pacific sector during ENSO episodes. *J. Climate,* **16,** 3–20.

——, and J. J. Ploshay, 2009: Simulation of synoptic- and subsynoptic-scale phenomena associated with the East Asian summer monsoon using a high-resolution GCM. *Mon. Wea. Rev.,* **137,** 137–160.

Lee, J.-Y., and B. Wang, 2012: Seasonal climate prediction and predictability of atmospheric circulation. *Climate Models,* L. M. Druyan, Ed., InTech, 19–42.

——, and Coauthors, 2010: How are seasonal prediction skills related to models' performance on mean state and annual cycle? *Climate Dyn.,* **35,** 267–283.

——, B. Wang, Q. Ding, K.-J. Ha, J.-B. Ahn, A. Kumar, B. Stern, and O. Alves, 2011: How predictable is the northern hemisphere summer upper-tropospheric circulation? *Climate Dyn.,* **37,** 1189–1203.

Li, T., and B. Wang, 2005: A review on the western North Pacific monsoon: Synoptic-to-interannual variabilities. *Terr. Atmos. Ocean. Sci.,* **16,** 285–314.

Livezey, R. E., 1995: Field intercomparison. *An Analysis of Climate Variability Applications of Statistical Techniques,* H. von Storch and A. Navara, Eds., Springer-Verlag, 159–175.

Lu, R., and Z. Lin, 2009: Role of subtropical precipitation anomalies in maintaining the summertime meridional teleconnection over the western North Pacific and East Asia. *J. Climate,* **22,** 2058–2072.

Luo, J.-J., S. Masson, S. Behera, S. Shingu, and T. Yamagata, 2005: Seasonal climate predictability in a coupled OAGCM using a different approach for ensemble forecasts. *J. Climate,* **18,** 4474–4497.

Matsueda, M., 2011: Predictability of Euro-Russian blocking in summer of 2010. *Geophys. Res. Lett.,* **38,** L06801, doi:10.1029/2010GL046557.

Metz, W., 1991: Optimal relationship of large-scale flow patterns and the barotropic feedback due to high-frequency eddies. *J. Atmos. Sci.,* **48,** 1141–1159.

Nakamura, H., and T. Fukamachi, 2004: Evolution and dynamics of summertime blocking over the Far East and the associated surface Okhotsk high. *Quart. J. Roy. Meteor. Soc.,* **130,** 1213–1233.

Ninomiya, K., 2009: Characteristics of precipitation in the Meiyu-Baiu season in the CMIP3 20th century climate simulations. *J. Meteor. Soc. Japan,* **87,** 829–843.

——, T. Nishimura, W. Ohfuchi, T. Suzuki, and S. Matsumura, 2002: Features of the Baiu front simulated in an AGCM (T42L52). *J. Meteor. Soc. Japan,* **80,** 697–716.

Nitta, T., 1987: Convective activities in the tropical western Pacific and their impact on the Northern Hemisphere summer circulation. *J. Meteor. Soc. Japan,* **65,** 373–390.

North, G. R., T. L. Bell, R. F. Cahalan, and F. J. Moeng, 1982: Sampling errors in the estimation of empirical orthogonal functions. *Mon. Wea. Rev.,* **110,** 699–706.

Onogi, K., and Coauthors, 2007: The JRA-25 Reanalysis. *J. Meteor. Soc. Japan,* **85,** 369–432.

Rayner, N. A., D. E. Parker, E. B. Horton, C. K. Folland, L. V. Alexander, D. P. Rowell, E. C. Kent, and A. Kaplan, 2003: Global analyses of sea surface temperature, sea ice, and night marine air temperature since the late nineteenth century. *J. Geophys. Res.,* **108,** 4407, doi:10.1029/2002JD002670.

Saha, S., and Coauthors, 2006: The NCEP Climate Forecast System. *J. Climate,* **19,** 3483–3517.

Sampe, T., and S.-P. Xie, 2010: Large-scale dynamics of the meiyu–baiu rainband: Environmental forcing by the westerly jet. *J. Climate,* **23,** 113–134.

Sato, N., and M. Takahashi, 2006: Dynamical processes related to the appearance of quasi-stationary waves on the subtropical jet in the midsummer Northern Hemisphere. *J. Climate,* **19,** 1531–1544.

Sohn, S.-J., Y.-M. Min, J.-Y. Lee, C.-Y. Tam, I.-S. Kang, B. Wang, J.-B. Ahn, and T. Yamagata, 2012: Assessment of the long-lead probabilistic prediction for the Asian summer monsoon precipitation (1983–2011) based on the APCC multimodel system and a statistical model. *J. Geophys. Res.,* **117,** D04102, doi:10.1029/2011JD016308.

Sui, C.-H., P.-H. Chung, and T. Li, 2007: Interannual and interdecadal variability of the summertime western North Pacific subtropical high. *Geophys. Res. Lett.,* **34,** L11701, doi:10.1029/2006GL029204.

Takaya, K., and H. Nakamura, 2001: A formulation of a phase-independent wave activity flux for stationary and migratory quasigeostrophic eddies on a zonally varying basic flow. *J. Atmos. Sci.,* **58,** 608–627.

Takaya, Y., T. Yasuda, T. Ose, and T. Nakaegawa, 2010: Predictability of the mean location of typhoon formation in a seasonal prediction experiment with a coupled general circulation model. *J. Meteor. Soc. Japan,* **88,** 799–812.

Tokinaga, H., and Y. Tanimoto, 2004: Seasonal transition of SST anomalies in the tropical Indian Ocean during El Niño and Indian Ocean dipole years. *J. Meteor. Soc. Japan,* **82,** 1007–1018.

Wakabayashi, S., and R. Kawamura, 2004: Extraction of major teleconnection patterns possibly associated with the anomalous summer climate in Japan. *J. Meteor. Soc. Japan,* **82,** 1577–1588.

Wang, B., I.-S. Kang, and J.-Y. Lee, 2004: Ensemble simulations of Asian–Australian monsoon variability by 11 AGCMs. *J. Climate,* **17,** 803–818.

——, Q. Ding, X. Fu, I.-S. Kang, K. Jin, J. Shukla, and F. Doblas-Reyes, 2005: Fundamental challenge in simulation and prediction of summer monsoon rainfall. *Geophys. Res. Lett.,* **32,** L15711, doi:10.1029/2005GL022734.

——, and Coauthors, 2009: Advance and prospectus of seasonal prediction: Assessment of the APCC/CliPAS 14-model ensemble retrospective seasonal prediction (1980–2004). *Climate Dyn.,* **33,** 93–117.

Watanabe, M., 2009: Self-limiting feedback between baroclinic waves and a NAO-like sheared zonal flow. *Geophys. Res. Lett.,* **36,** L08803, doi:10.1029/2009GL037176.

——, and M. Kimoto, 2000: Atmosphere–ocean thermal coupling in the North Atlantic: A positive feedback. *Quart. J. Roy. Meteor. Soc.,* **126,** 3343–3369; Corrigendum, **127,** 733–734.

Wu, B., T. Zhou, and T. Li, 2009: Seasonally evolving dominant interannual variability modes of East Asian climate. *J. Climate,* **22,** 2992–3005.

——, T. Li, and T. Zhou, 2010: Relative contributions of the Indian Ocean and local SST anomalies to the maintenance of the western North Pacific anomalous anticyclone during the El Niño decaying summer. *J. Climate,* **23,** 2974–2986.

Wu, R., and B. Kirtman, 2007: Regimes of seasonal air-sea interaction and implications for performance of forced simulations. *Climate Dyn.,* **29,** 393–410.

Xie, P., and P. A. Arkin, 1997: Global precipitation: A 17-year monthly analysis based on gauge observations, satellite estimates, and numerical model outputs. *Bull. Amer. Meteor. Soc.,* **78,** 2539–2558.

Xie, S.-P., H. Annamalai, F. A. Schott, and J. P. McCreary, 2002: Structure and mechanisms of south Indian Ocean climate variability. *J. Climate,* **15,** 864–878.

——, K. Hu, J. Hafner, H. Tokinaga, Y. Du, G. Huang, and T. Sampe, 2009: Indian Ocean capacitor effect on Indo–western Pacific climate during the summer following El Niño. *J. Climate,* **22,** 730–747.

Yang, J., Q. Liu, S.-P. Xie, Z. Liu, and L. Wu, 2007: Impact of the Indian Ocean SST basin mode on the Asian summer monsoon. *Geophys. Res. Lett.,* **34,** L02708, doi:10.1029/2006GL028571.

Yasui, S., and M. Watanabe, 2010: Forcing processes of the summertime circumglobal teleconnection pattern in a dry AGCM. *J. Climate,* **23,** 2093–2114.

Zhong, A., H. H. Hendon, and O. Alves, 2005: Indian Ocean variability and its association with ENSO in a global coupled model. *J. Climate,* **18,** 3634–3649.

Zhou, T., B. Wu, and B. Wang, 2009: How well do atmospheric general circulation models capture the leading modes of the interannual variability of the Asian–Australian monsoon? *J. Climate,* **22,** 1159–1173.